Journal of Magnetism and Magnetic Materials 68 (1987) 335–343
North-Holland, Amsterdam

ANGULAR DEPENDENCE OF THE COERCIVE FORCE OF TEXTURED RARE EARTH PERMANENT MAGNETS

L. JAHN, K. ELK and R. SCHUMANN

Hochschule für Verkehrswesen "Friedrich List", Wissenschaftsbereich Physik, Dresden, German Dem. Rep.

Received 30 December 1986; in revised form 27 April 1987

On the basis of model calculations experimental results on the angular dependence of the coercivity H_c and the remanence coercivity H_R of hard magnetic materials of the type $SmCo_5$, $Sm_2(Co, Fe, Cu, Zr)_{15}$ and $Nd_2Fe_{14}B$ are discussed. In the model coherent rotation as well as incoherent magnetization jumps (e.g. 180°-Bloch walls) are included. The texture is described by an axial symmetric distribution of the easy axes with only one parameter. For $Sm_2(Co, Fe, Cu, Zr)_{15}$ the model explains irreversible ($H_R(\theta)$-curves) as well as reversible ($H_R(\theta) - H_c(\theta)$) magnetization processes in good agreement with the experiments, whereas stronger deviations exist for $SmCo_5$ and $Nd_2Fe_{14}B$, especially in the $H_c(\theta)$-curves. These deviations should be caused by other reversible magnetization processes.

1. Introduction

Anisotropic polycrystalline permanent magnets show a strong dependence of the remanent magnetization $\boldsymbol{J}_R$ and the coercive force H_c on the angle θ between the direction of the applied field $\boldsymbol{H}$ and the texture axis $\boldsymbol{t}$. By a detailed investigation of this angle dependence it is possible to get information on the mechanism of magnetization reversal in magnetic materials.

At present the most important hard magnetic materials (with the highest values of the energy product) are $SmCo_{5-x}$ [1,2] (type A), $Sm_2(Co, Fe, Cu, Zr)_{17-x}$ [3,4] (type B), and $Nd_2Fe_{14}B$ [5,6] (type C). At room temperature they all show high values of the crystal anisotropy constant K_1 ($K_1 > J_s^2/\mu_0$, where J_s is the saturation magnetization) and of the coercivity H_c ($H_c > J_s/\mu_0$ at $\theta = 0$).

To calculate the magnetization coercivity H_c ($=_j H_c$) and the remanence coercivity H_R the mechanism of the magnetization reversal of the single crystal has to be known. For the above mentioned materials coherent rotation [7,8] and incoherent wall shift processes [9,10] are assumed to be of importance. Following Kondorsky [11] the angle dependence of H_c of single crystals due to irreversible jumps of 180°-Bloch walls (denoted in the following by K) can be described by

$$H_c^K(\vartheta) = H_R^K(\vartheta) = H_c^0/\cos\vartheta, \tag{1}$$

where H_c^0 denotes the coercive force for single crystals with fields parallel to the easy axis (with $H_c^0 \ll H_A = 2K_1/J_s$ in general). The contribution of coherent rotation processes [7,8] (denoted by SW) can be calculated by minimizing the magnetic part of the free energy containing the anisotropy energy $K_1 \sin^2\varphi$ and the field energy $HJ_s \cos(\vartheta - \varphi)$. (For definition of the angles see fig. 1.) For single crystals the angular dependences of H_R and H_c due to coherent rotation processes are given by

$$H_R^{SW}(\vartheta) = H_A(\cos^{2/3}\vartheta + \sin^{2/3}\vartheta)^{-3/2} \tag{2}$$

and

$$H_c^{SW}(\vartheta) = \begin{cases} H_R^{SW}(\vartheta) \\ (H_A/2)\sin 2\vartheta \end{cases} \quad \text{if } \vartheta \lessgtr \pi/4, \tag{3}$$

respectively. It should be noticed that due to $H_c^0 \ll H_A$ these rotation jumps are of influence only at large angles (fig. 2).

Other often discussed contributions to the magnetization reversal like curling [12] in materials with shape anisotropy or considerations related to

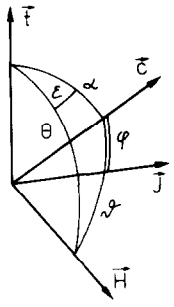

Fig. 1. Definition of the used angles. t – texture axis, H – applied magnetic field, c – easy direction, J – magnetization of a given crystallite.

elongated single domain particles [13] and AlNiCo [14] as well as the influence of interaction [15] are neglected in the model discussed in section 2.

In the following the dependence of H_c and H_R on θ is calculated for a polycrystalline textured magnet using a model containing K- and SW-processes and generalizing the calculations of H_c and H_R at $\theta = 0$ [16,17]. Thereby $H_c(\theta)$ and $H_R(\theta)$ follow from the numerical computation of

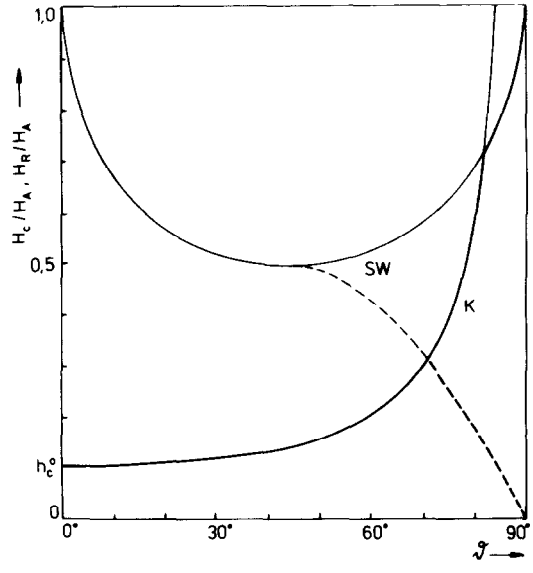

Fig. 2. Angular dependence of the critical fields $H_R(\theta)$ (full lines) and $H_c(\theta)$ (dashed line) of a single crystal (with $H_c^0 = 0.1H_A$). Fat lines denote the resulting curves. K – incoherent jumps, SW – coherent rotation.

the angular dependent hysteresis loops of magnetization and remanence [18]. Furthermore experimental results of samples of the types A, B and C are reported and discussed by comparison with the model calculations. Especially the maximum of $H_c(\theta)$, known from ferrites but not observed in MnAlC [19], as well as the dependence of $H_c(\theta)$ and $H_R(\theta)$ on the angle between saturation and measuring fields are considered to give information on the reversible part of the magnetization reversal processes.

2. Calculation of $H_c(\theta)$ and $H_R(\theta)$

2.1. The model

To calculate the angle dependence of H_c and H_R a model is used consisting of identical particles with uniaxial anisotropy, where the distribution of the easy axes is described by an axial symmetric texture function [20,21]

$$f(\alpha) = (2n + 1)\cos^{2n}\alpha \qquad (4)$$

with only one texture parameter n. The single particles of the polycrystalline sample can change their magnetization direction by incoherent wall shifts (K) as well as coherent rotation (SW).

The magnetization J of the sample follows by averaging the particle magnetizations on the texture function (4). Thereby the components of J parallel and perpendicular to the applied field H, $J_\parallel$ and $J_\perp$, resp., result from a numerical procedure described in ref. [18] in detail. In the same manner the remanent magnetization J_R and its components $J_{R\parallel}$ and $J_{R\perp}$ are obtained by switching off H before the averaging on $f(\alpha)$ is carried out, i.e. there are only irreversible changes of the magnetization left. As a result of this procedure one gets J, J_R and their components as functions of the field strength H, the field direction θ, and the texture parameter n.

The coercivity H_c is given by the condition $J_\parallel = 0$, starting from a well defined initial state (saturation with a field $H_S > H_A$ in the direction θ_S) and applying a field H_M in the direction θ_M. Analogously H_R is given by $J_{R\parallel} = 0$. Hence H_c and H_R are functions of θ_M, θ_S and n.

2.2. Numerical results

In agreement with the experimental situation 3 different combinations of the saturation angle θ_S and the measuring angle θ_M are considered:

$$\begin{aligned} &(1)\quad \theta_S = \theta, \quad \theta_M = \theta + \pi, \\ &(2)\quad \theta_S = 0, \quad \theta_M = \theta + \pi, \\ &(3)\quad \theta_S = \theta, \quad \theta_M = \pi. \end{aligned} \tag{5}$$

Corresponding to these choices 3 different plots for $H_c(\theta)$ and $H_R(\theta)$ are obtained.

In the numerical calculations for simplicity only a fixed value of H_c^0 has been chosen ($H_c^0 = 0.1 H_A$ in agreement with ref. [18]). Contrary to this assumption in real systems usually a H_c^0-distribution exists. The influence of reasonable distributions is discussed in ref. [22] and should be rather small. Likewise the dependence of H_c^0 on the field H_S, which is of importance in some rare earth magnets, can be neglected since the initial state is assumed to be saturated completely.

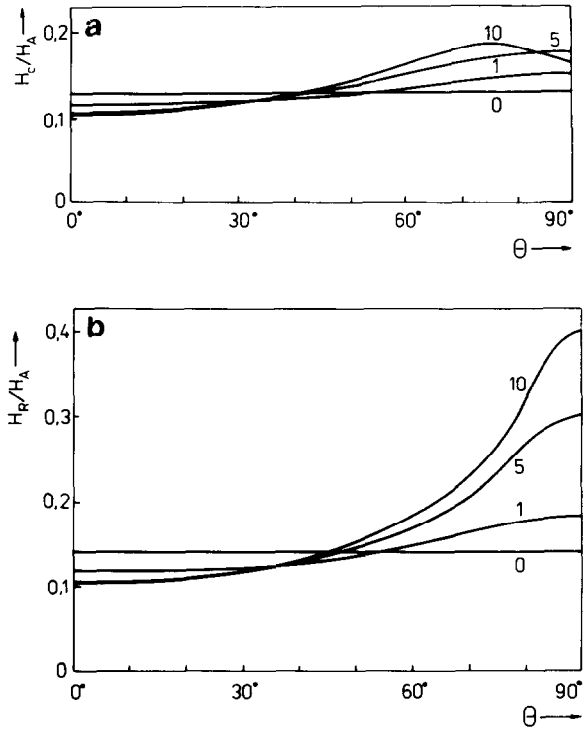

Fig. 3. Numerical results of the used model for case (1) of (5) with the texture parameters $n = 0$, 1, 5 and 10. a) $H_c(\theta)$, b) $H_R(\theta)$.

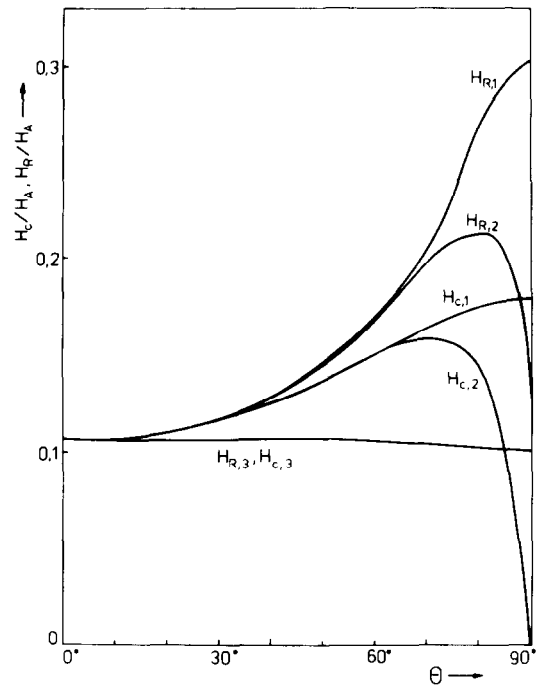

Fig. 4. Model results for $H_c(\theta)$ and $H_R(\theta)$ with $n = 5$ for all three combinations of the saturation and the measuring direction, defined in (5).

Fig. 3 presents the computed result for $H_c(\theta)$ and $H_R(\theta)$ for the combination (1) of eq. (5). At small values of the texture parameter n the coercivity H_c increases weakly with θ. A maximum is obtained only at higher values of n. On the other hand H_R increases monotonously already at bad textures. In fig. 4 $H_c(\theta)$ and $H_R(\theta)$ are plotted for $n = 5$ and all three combinations of (5). It is significant that the values of H_c and H_R of the combination (1) are always the highest ones, whereas the results obtained in case (3) are always smaller than those of (2), except the H_c values at very large angles.

2.3. Analytical relations

Within the considered model for case (1) of (5) the remanence coercivity H_R can be calculated analytically for the easy and hard direction, i.e.

$\theta = 0$ and $\theta = \pi/2$, respectively. In agreement with the experimental situation only the region

$$h_c^0 = H_c^0/H_A < \sqrt{2}/4 \tag{6}$$

is considered here. (Analogous expressions are possible for higher values of H_c^0 too [23].) From $J_{R\parallel} = 0$ it follows

$$H_R(0) = \sqrt[2n+2]{2}\, H_c^0 \tag{7}$$

and

$$H_R(\pi/2) = \begin{cases} H_c^0\left(1 - \sqrt[n+1]{0.5}\right)^{-1/2} \\ H_A \sqrt[2n+2]{2} \Big/ \left[\sqrt[3]{\sqrt[n+1]{2} - 1} + 1\right]^{3/2} \end{cases}$$

$$\text{if} \quad n \lessgtr n_g, \tag{8}$$

where

$$n_g = \ln 2 / \ln\left[\left(\left(1/h_c^0\right)^{2/3} - 1\right)^{-3} + 1\right] - 1. \tag{9}$$

Comparing (7) and (8) a possibility is given for the experimental determination of the texture parameter n by measuring the quotient

$$\beta(n) = \frac{H_R(\pi/2)}{H_R(0)} = \begin{cases} \left(\sqrt[n+1]{2} - 1\right)^{-1/2} \\ \dfrac{1}{h_c^0}\left(\sqrt[3]{\sqrt[n+1]{2} - 1} + 1\right)^{-3/2} \end{cases}$$

$$\text{if} \quad n \lessgtr n_g. \tag{10}$$

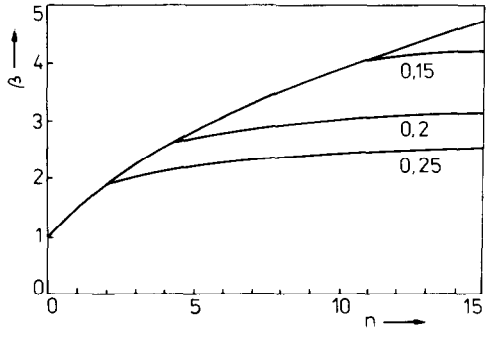

Fig. 5. Calculated dependence of the quotient $\beta(n)$ on the texture parameter n for different values of h_c^0.

In fig. 5, $\beta(n)$ is plotted in the interesting region $0 \leqslant n < 15$.

3. Experiments

In the hard magnetic materials mentioned above (Types A, B and C) the magnetization reversal is governed by quite different elementary processes which in general cannot be reduced to coherent rotation and incoherent wall jumps alone. But nevertheless a comparison of experimental magnetization curves with the computed results presented above should give some information on the range of validity of the model [18] as well as on additional processes which for a given material should be taken into account.

3.1. Samples, saturation and measurement

For the investigated mostly commercial (except the casting alloy) samples the magnetic parameters at room temperature are given in table 1. From these materials disks have been cut (diameter 4 mm, thickness 1 mm) with the texture axis within the disk plane. The measurements were carried out in the open circuit using a vibrating sample magnetometer (VPM) [24] with varying angle $\theta(\Delta\theta = \pm 0.1°)$ and variable temperature ($\Delta T = \pm 1$ K) and a maximum field $\mu_0 H_{max} = 1.1$ T.

Most of the measurements were performed at higher temperatures T_m to keep $\mu_0 H_R(\pi/2) < 1.1$ T. The coercivity H_c is reached if the signal vanishes. Then to measure the remanence coercivity H_R the field was stepwise increased and switched off until the remanent signal in the VPM goes to 0. For the saturation of the samples mounted in the VPM a "thermomagnetic method" was used where with an applied maximum field H_{max} the temperature was increased from T_m to T_{max} (table 1) for a time of 3 s. For checking of the method the samples were saturated outside of the VPM in a pulsed field ($\mu_0 H = 10$ T, $\Delta\theta = \pm 2°$). The texture axis ($\theta = 0$) was determined by the condition that the remanence J_R is parallel to the applied field.

Table 1
Magnetic parameters B_R, $H_c(0)$ and $(BH)_{max}$ at room temperature, texture parameter n, saturation field H_{max} at T_{max}, measuring temperature T_m, reduced coercivity $\bar{h}_c$ at T_m and quotient $\beta(n)$

Material	B_R (T)	$\mu_0 H_c(0)$ (T)	$(BH)_{max}$ 10^4 Wsm^{-3}	n	T_{max} (°C)	$\mu_0 H_{max}$ (T)	T_m (°C)	$\bar{h}_c(T_m)$	$\beta_{exp}(n)$	$\beta_{th}(n)$
(A) $SmCo_5$										
sintered (RECOMA 20) [a]	0.9	> 2	15	4.5	610	1.1	387 447	0.017 0.010	3.3	2.73
sintered (KC 37) [a]	0.7	> 2	11	0.7	610	1.1	402	0.015	1.67	1.41
(B) $Sm(Co_{0.65}Fe_{0.27}Cu_{0.06}Zr_{0.02})_{7.44}$										
sintered (TOHOKU-Met 23) [a]	1.1	1.0	24	12	600	1.1	520 505	0.07 0.08	3.24	4.27
casting [b]	0.6	0.26	4	≈ 0	20	2.8	20	0.04	1.05	1
powder (isotr.)	0.3	0.37	1.5	0	20	2.8	20	0.04	1.0	1
powder (anis.)	0.6	0.32	2.5	4	20	2.8	20	0.04	2.0	2.6
(C) $Nd_2Fe_{14}B$										
sintered (NERONIT 240) [a]	1.25	1.5	26.5	1.5	300	1.1	108	0.17	1.4	1.77

[a] Trade name.
[b] O_2-content < 0.1 wt%, vacuum heat treated: 3 h at 1170 °C, 15 h at 830 °C, cooling: 15 h to 400 °C.

3.2. Determination of the texture and check on the saturation

By generalization of the method described in refs. [20,21] the angular dependence of the remanence direction

$$\gamma(\theta) = \theta - \arctan\left(J_{R\perp}(\theta)/J_{R\parallel}(\theta)\right) \qquad (11)$$

was investigated. This has two advantages: (i) It is not necessary to determine the absolute value of the saturation magnetization and (ii) by checking the condition $\gamma(\pi/2) = \pi/2$, fulfilled only for completely saturated materials [18], it is possible to control the saturation of the sample. Finally comparing the measured values of $\gamma(\theta)$ with theoretical calculations [18,25] the texture parameter n can be determined.

3.3. Experimental results

Figs. 6–11 show the dependence of H_c and H_R on the angle θ at different temperatures, considering the three combinations of saturation and measuring directions described in (5). Further-

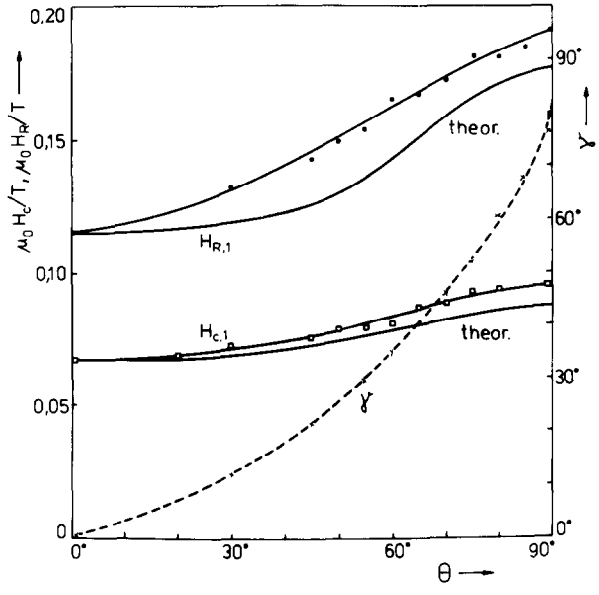

Fig. 6. Measured values of $H_{c,1}(\theta)$ and $H_{R,1}(\theta)$ (case (1) of (5)) for $SmCo_5$ (sintered magnet with $n = 0.7$ and $\bar{h}_c = 0.015$) and comparison with theoretical results ($n = 1$, $h_c^0 = 0.1$, fitted at $\theta = 0$).

more, for the combination (1), experimental values of $\gamma(\theta)$ are presented demonstrating that the saturation of the samples was approximately reached.

As discussed above, in most cases the measurements were carried out at higher temperatures. Since the single particle coercivity h_c^0 is not known in general, for comparison of theoretical and experimental curves the temperature dependent parameter

$$\bar{h}_c(T) = H_c(0;\, T)/H_A(T), \qquad H_A(T) = 2K_1(T)/J_s(T) \tag{12}$$

was used. Of course, for bad textures $\bar{h}_c$ differs from h_c^0, but it gives the right order of magnitude. The parameters $J_s(T)$ and $K_1(T)$ have been taken from the literature [26–28].

In the figs. 6, 8, 9 and 11 the theoretical curves of H_c and H_R was fitted to the experiments at $\theta = 0$.

3.3.1. $SmCo_5$ (A)

Although the parameter $\bar{h}_c$ is much smaller than the value 0.1 assumed for h_c^0 in the model calculations, the monotonous increasing of $H_{R,1}(\theta)$ (fig. 6) is in correspondence with the Kondorsky assumption (1) for the description of the irreversible wall shifts. Furthermore assuming the texture parameter to be $n = 0.7$ the monotonous increasing of $H_{c,1}(\theta)$ is in good agreement with the theoretically calculated curves, whereas the measured value of the quotient $\beta(n)$, however, is higher than that one following from (10). The large difference $H_{R,1}(\theta) - H_{c,1}(\theta)$ cannot be explained within the considered model.

For a sample with a higher degree of texture, the three measured $H_c(\theta)$-curves for two temperatures T_m are plotted in fig. 7. It is remarkable that for intermediate values of θ one gets $H_{c,2}(\theta) > H_{c,1}(\theta)$. That hints at additional reversible magnetization processes. On the other hand, except at large angles, $H_{c,3}(\theta)$ shows the expected behaviour. Finally it should be mentioned that at $\theta \approx 70°$ $H_{R,2}(\theta)$ (not plotted in the figure) is greater than $H_{R,1}(\theta)$ too.

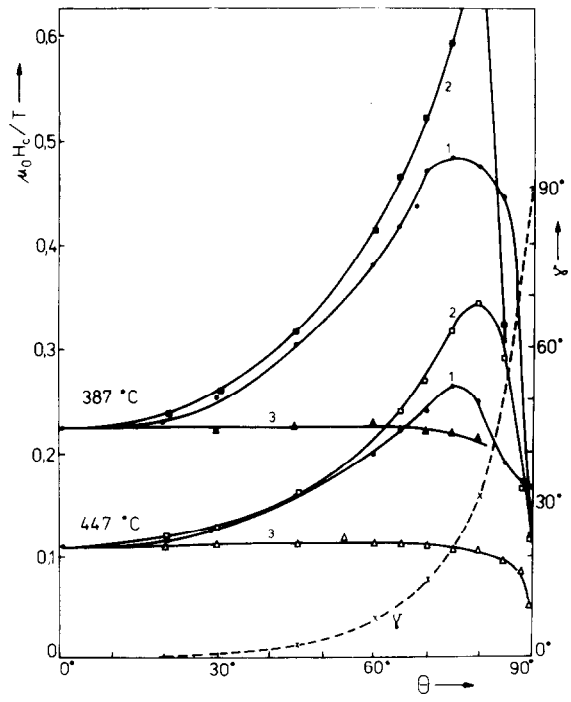

Fig. 7. Comparison of $H_{c,1}(\theta)$, $H_{c,2}(\theta)$ and $H_{c,3}(\theta)$ for $SmCo_5$ ($n = 4.5$) at $T_m = 387\,°C$ ($\bar{h}_c(T_m) = 0.017$) and $T_m = 447\,°C$ ($\bar{h}_c(T_m) = 0.010$). Additionally $\gamma(\theta)$ is plotted.

3.3.2. $Sm_2(Co, Fe, Cu, Zr)_{15}$ (B)

The sintered magnets investigated at high temperatures as well as the cast and powder samples studied at room temperatures show the best qualitative agreement with the predictions of the considered model. For example the maximum of $H_{c,1}(\theta)$ was measured for well textured magnets (fig. 8), although the absolute values are smaller than the calculated ones. This statement is valid for $H_{R,1}(\theta)$ too. Of course, for the nearly isotropic cast sample with a high density and the less compact isotropic powder magnet, the $H_{c,1}$- and $H_{R,1}$-values do not show any angular dependence. However, for the case (2) of eq. (5) a dependence on θ exists, in agreement with the theory. Fig. 9 shows that in the lower and intermediate region of θ the monotonous decrease is in rather good agreement with the theoretical behaviour, whereas deviations occur at higher angles, especially for $H_{R,2}(\theta)$.

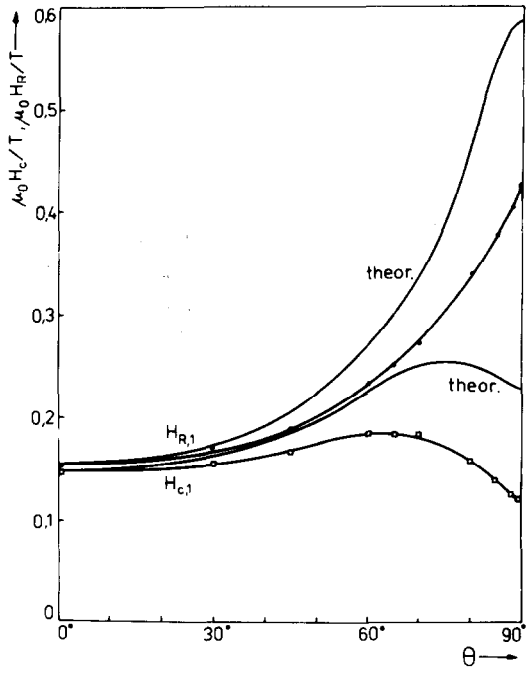

Fig. 8. Sintered $Sm_2(Co, Fe, Cu, Zr)_{15}$-magnet with $n = 12$ and $\bar{h}_c = 0.07$, measured at $T_m = 520\,°C$. The theoretical curves are fitted at $\theta = 0$ ($n = 10$, $h_c^0 = 0.1$).

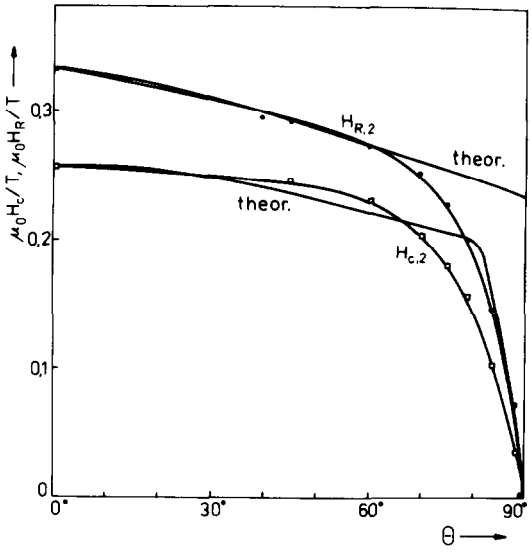

Fig. 9. $H_{c,2}(\theta)$ and $H_{R,2}(\theta)$ for an isotropic cast sample of $Sm_2(Co, Fe, Cu, Zr)_{15}$ with $\bar{h}_c = 0.04$.

For the anisotropic samples the figs. 10a (powder magnet, investigated at room temperature) and 10b (sintered magnet at $T_m = 505\,°C$) show that the magnetization processes can be well described within the given model. At all angles the relations $H_{c,1}(\theta) > H_{c,2}(\theta) > H_{c,3}(\theta)$ and $H_{R,1}(\theta)$

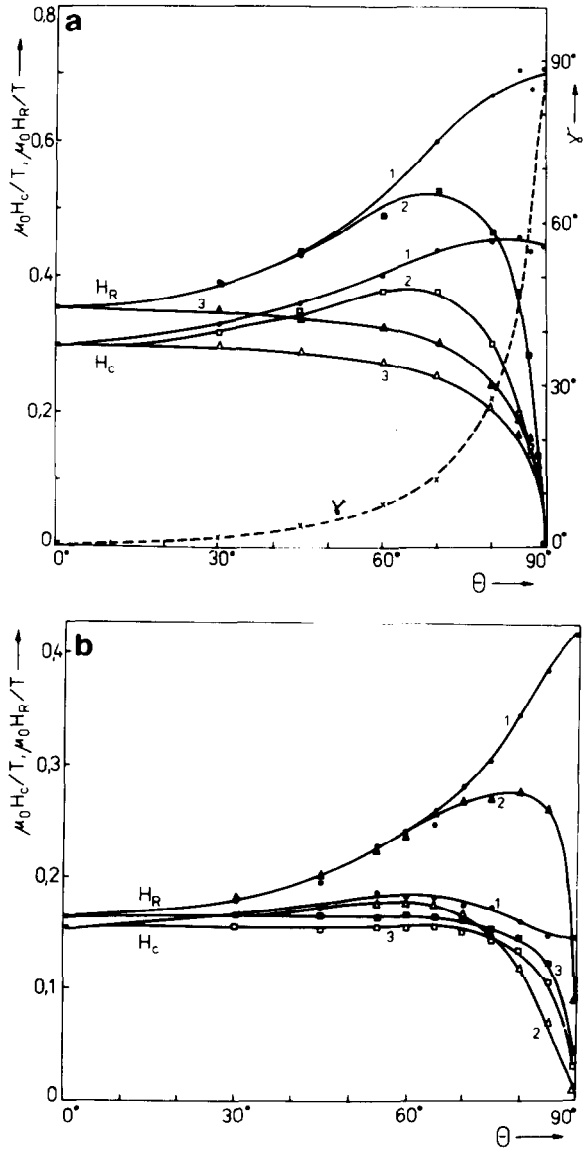

Fig. 10. $H_c(\theta)$ and $H_R(\theta)$ for anisotropic samples of $Sm_2(Co, Fe, Cu, Zr)_{15}$ for different combinations of saturation and measuring direction. a) powder magnet ($n = 4$, $\bar{h}_c = 0.04$, $T_m = 20\,°C$), b) sintered magnet ($n = 12$, $\bar{h}_c = 0.08$, $T_m = 505\,°C$).

$> H_{R,2}(\theta) > H_{R,3}(\theta)$ are fulfilled. At $\theta = 0$ the difference between H_c and H_R is larger for the powder sample than for the sintered one.

3.3.3. $Nd_2Fe_{14}B$ (C)

Similar to $SmCo_5$ (fig. 6), fig. 11 shows a large difference between $H_R(0)$ and $H_c(0)$ hinting at relatively high contributions of reversible magnetization processes. The monotonous increasing of $H_{R,1}(\theta)$ corresponds to the small texture parameter $n = 1.5$. However, in contradiction to $SmCo_5$ for this material we find $\beta_{exp} < \beta_{th} = 1.77$, following from (10).

For all three $H_c(\theta)$-curves there are remarkable differences between theoretical and experimental results. The $H_{c,1}(\theta)$-plot shows a strong decrease at large angles with a very flat maximum. Furthermore the high values of $H_{c,2}(\theta)$ and the behaviour of $H_{c,3}(\theta)$ are contrary to the theoretical predictions. Additionally, similar to $SmCo_5$, a distinct maximum of $H_{R,2}(\theta)$ exists for intermediate values of θ.

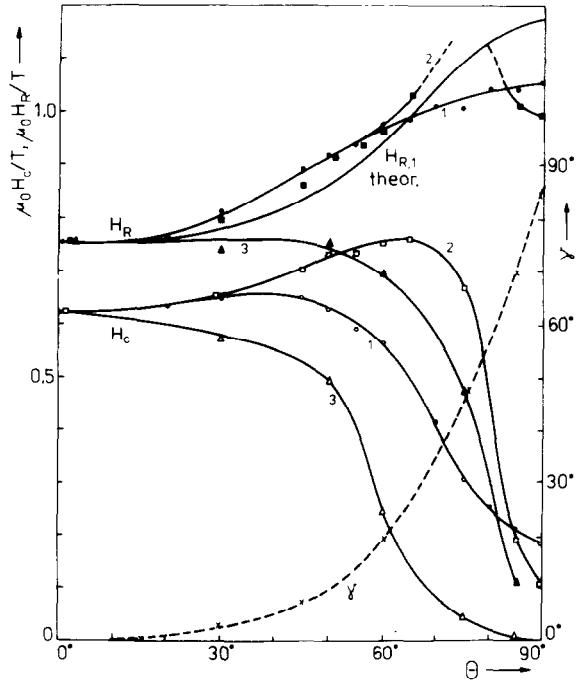

Fig. 11. Sintered $Nd_2Fe_{14}B$-magnet ($n = 1.5$, $\bar{h}_c = 0.17$, $T_m = 108\,°C$). $H_c(\theta)$ and $H_R(\theta)$ measured for all three cases of (5). The theoretical curve ($n = 1$, $h_c^0 = 0.1$) is fitted at $\theta = 0$.

4. Discussion

The comparison of the experimental data of section 3 with the theoretical results (section 2) shows, that the used simple model explains the qualitative behaviour of $Sm_2(Co, Fe, Cu, Zr)_{15}$ (group B) rather well. Therefore it can be concluded that the volume-pinning and the nearly irreversible shift of the Bloch walls in these materials [29–31] can be described sufficiently by (1).

On the other hand, distinct deviations from the model are obtained for materials of the groups A and C, in which the coercivity is so-called "nucleation controlled". Especially the strong decrease of $H_c(\theta)$ at large angles and the observed order of the values of $H_c(\theta)$ and $H_R(\theta)$ for different relations between saturation and measuring direction are not in agreement with the presented theory. Also a partial similarity to shape anisotropic materials [13,14] in the $H_c(\theta)$-plots of the group C-materials is of interest.

A possible explanation of the observed deviations of the materials A [2,29,32] and C [5,33,34] should be given by the assumption that the magnetic hardness of these material is caused by the existence of distinct phases at the grain boundaries, investigated in $SmCo_5$ [32] and $Nd_2Fe_{14}B$ [34]. Such local defect centers can produce a nonsymmetric contribution to (1) as observed in single crystals [35]. Furthermore additional reversible magnetization processes as, e.g., reversible wall shifts should be taken into account which are more likely to explain the large difference between $H_R(0)$ and $H_c(0)$ than the coherent rotation process.

However, the irreversible wall shift processes described by (1) are responsible for the hysteresis in $SmCo_5$ and $Nd_2Fe_{14}B$, too. This follows from the monotonous increase of $H_{R,1}(\theta)$ with θ and the texture parameter n. That increase hints at the same $(1/\cos \vartheta)$-law as known from measurements on single crystals of $SmCo_5$ [35,36] and Sr-ferrites [37].

Acknowledgement

The authors are greatly indebted to Dr. V. Christoph for valuable hints and discussions.

References

[1] K.J. Strnat, Z. Kobalt 36 (1967) 119.
[2] K.S.V.L. Narasimhan, J. Appl. Phys. 52 (1981) 2512.
[3] T. Ojima, S. Tomizawa, T. Yoneyama and T. Hori, IEEE Trans. Magn. MAG-13 (1977) 1317.
[4] R.K. Mishra and G. Thomas, Proc. IV Intern. Workshop RE–Co magnets, Hakone, Japan (1979).
[5] M. Sagawa, S. Fujimura, N. Togawa, H. Yamemoto and Y. Matsuura, J. Appl. Phys. 55 (1984) 2083.
[6] Bao-Min Ma and K.S.V.L. Narasimhan, J. Magn. Magn. Mat. 54–57 (1986) 559.
[7] E.C. Stoner and E.P. Wohlfarth, Phil. Trans. Roy. Soc. A 240 (1948) 599.
[8] E.P. Wohlfarth, J. Appl. Phys. Suppl. 30 (1960) 117 S.
[9] J.D. Livingston, J. Appl. Phys. 53 (1981) 2544.
[10] J.D. Livingston, J. Appl. Phys. 57 (1985) 4137.
[11] E.J. Kondorsky, J. Exp. Theor. Fiz. 10 (1940) 420.
[12] S. Shtrikman and D. Treves, J. Phys. Rad. 20 (1959) 286.
[13] F.E. Luborsky and T.O. Paine, J. Appl. Phys. Suppl. 31 (1960) 66 S.
[14] E.P. Wohlfarth, in: Ferromagnetic Materials (North-Holland, Amsterdam, 1982).
[15] R. Straubel and D. Robaschik, Phys. Stat. Sol. 16 (1966) 237.
[16] L. Jahn, R. Schumann and V. Christoph. Phys. Stat. Sol. (a) 88 (1985) 595.
[17] R. Schumann and L. Jahn, Elektrie 40 (1986) 306.
[18] K. Elk and V. Christoph, J. Magn. Magn. Mat. 65 (1987) 151.
[19] L. Jahn, U. Heinecke and D. Hinz, Hermsdorfer Techn. Mitteil. 25 (1985) 2160.
[20] S. Shtrikman and D. Treves, J. Appl. Phys. Suppl. 31 (1960) 58 S.
[21] H. Stäblein and J. Willbrand, Z. Angew. Phys. 32 (1971) 70.
[22] K. Elk and V. Christoph, Phys. Stat. Sol. (a) 98 (1986) K 53.
[23] K. Elk, V. Christoph, L. Jahn and R. Schumann, Wiss. Z. HfV 34 (1987) 481.
[24] S. Foner, Rev. Sc. Instr. 46 (1975) 1425.
[25] L. Jahn, R. Schumann and W. Lange, Wiss. Z. HfV 34 (1987) 143.
[26] H.P. Klein and A. Menth, AIP Conf. Proc. 18 (1974) 1177.
[27] H.P. Klein, A. Menth and R.S. Perkins, Physica 80B (1975) 153.
[28] R. Grössinger, X.K. Sun, R. Eibler and H.R. Kirchmayr, in: Proc. 8th Workshop RE-Magnets, Dayton, Ohio 1985, p. 553.
[29] J.D. Livingston, J. Appl. Phys. 52 (1981) 2544.
[30] H. Kronmüller, K.-D. Durst, W. Ervens and W. Ferengel, IEEE Trans. Magn. MAG-20 (1984) 1569.
[31] D. Li and K.J. Strnat, J. Appl. Phys. 55 (1984) 2103.
[32] K. Kuntze, Dissertation, Göttingen (1981).
[33] D. Li and K.J. Strnat, J. Appl. Phys. 57 (1985) 4143.
[34] K.-D. Durst and H. Kronmüller, J. Magn. Magn. Mat. 59 (1986) 86.
[35] A.J. Ulyanov, Izv. Akad. Nauk 45 (1981) 1695.
[36] A.J. Ulyanov, A.V. Deryagin and G.S. Kandaurova, Phys. Stat. Sol. (a) 26 (1974) K 167.
[37] U. Heinecke and L. Jahn, Phys. Stat. Sol (a) 10 (1972) K 93.